Electronic Supplementary Material (ESI) for *Dalton Trans.*

Syntheses, Structures and Magnetic Properties of Lanthanide Complexes of the Pyrimidyl-Substituted Nitronyl Nitroxide Radical

Jian Wang,[a] Hao Miao,[a] Zhao-Xin Xiao,[a] Yan Zhou,[a] Lin-Dan Deng,[a] Yi-Quan Zhang*[b] and Xin-Yi Wang*[a]

[a] *State Key Laboratory of Coordination Chemistry, Collaborative Innovation Center of Advanced Microstructures, School of Chemistry and Chemical Engineering, Nanjing University, Nanjing, 210023, China. Fax:+86-25-83314502. E-mail: wangxy66@nju.edu.cn*

[b] *Jiangsu Key Laboratory for NSLSCS, School of Physical Science and Technology, Nanjing Normal University, Nanjing 210023, China. E-mail: zhangyiquan@njnu.edu.cn*

Supporting Information

Table of contents

1. X-ray crystallography and powder x-ray diffraction

Table S1. Selected bond lengths [Å] and angles [°] for complexes **1-4**.

	1$_{Tb}$	**2**$_{Dy}$	**3**$_{Ho}$	**4**$_{Er}$
Ln1-O1	2.306(3)	2.302(2)	2.281(3)	2.270(3)
Ln1-O3	2.327(3)	2.312(2)	2.304(3)	2.287(3)
Ln1-O4	2.382(3)	2.368(2)	2.365(4)	2.328(3)
Ln1-O5	2.371(4)	2.356(3)	2.352(4)	2.325(4)
Ln1-O6	2.325(3)	2.308(3)	2.299(4)	2.275(3)
Ln1-O7	2.339(3)	2.329(2)	2.317(3)	2.274(3)
Ln1-O8	2.377(3)	2.357(2)	2.355(4)	2.331(3)
Ln1-N3	2.632(4)	2.618(3)	2.614(4)	2.595(4)
O1-Ln1-O3	97.33(11)	97.76(8)	97.26(11)	144.68(12)
O1-Ln1-O4	71.41(11)	71.48(8)	70.90(12)	81.42(12)
O1-Ln1-O5	143.33(12)	142.97(9)	143.14(12)	143.04(13)
O1-Ln1-O6	86.36(12)	85.13(9)	85.92(12)	85.89(14)
O1-Ln1-O7	143.66(10)	144.08(8)	144.37(12)	96.01(14)
O1-Ln1-O8	81.28(10)	81.28(8)	81.09(11)	70.56(13)
O1-Ln1-N3	69.85(11)	70.23(8)	70.45(11)	70.65(12)
O3-Ln1-O4	72.23(11)	72.52(8)	72.92(12)	74.15(12)
O3-Ln1-O5	83.81(11)	84.04(9)	83.36(12)	72.25(14)
O3-Ln1-O6	143.68(12)	144.11(8)	144.32(12)	110.06(13)
O3-Ln1-O7	88.77(11)	88.15(8)	88.06(12)	88.44(12)
O3-Ln1-O8	142.42(11)	142.42(8)	142.42(11)	143.13(12)
O3-Ln1-N3	73.16(11)	73.18(8)	72.85(11)	77.45(13)
O4-Ln1-O5	74.18(12)	73.95(9)	74.19(13)	120.41(14)
O4-Ln1-O6	74.89(12)	74.65(9)	74.71(12)	72.84(13)
O4-Ln1-O7	143.37(11)	142.89(8)	143.13(13)	142.36(12)
O4-Ln1-O8	139.39(12)	139.34(8)	138.46(12)	137.77(12)
O4-Ln1-N3	123.05(11)	123.40(8)	123.46(12)	71.18(12)
O5-Ln1-O6	72.69(13)	73.26(9)	73.71(13)	74.56(14)
O5-Ln1-O7	72.83(11)	72.74(9)	72.41(13)	83.56(13)
O5-Ln1-O8	119.26(12)	118.97(8)	119.98(12)	74.02(15)
O5-Ln1-N3	142.93(12)	143.16(9)	142.17(12)	141.69(12)
O6-Ln1-O7	109.40(11)	110.28(8)	109.78(12)	144.73(13)
O6-Ln1-O8	73.89(12)	73.46(8)	73.25(12)	74.20(13)
O6-Ln1-N3	140.05(12)	139.30(8)	139.77(12)	139.33(12)
O7-Ln1-O8	72.64(10)	73.06(8)	73.77(12)	73.34(12)
O7-Ln1-N3	77.92(11)	77.86(8)	77.71(12)	72.58(12)
O8-Ln1-N3	71.19(11)	71.21(8)	71.29(11)	124.21(12)

Table S2. Selected bond lengths [Å] and angles [°] for complexes **5-8**.

	5$_{Tb}$	**6**$_{Dy}$	**7**$_{Ho}$	**8**$_{Er}$
Ln1-O1	2.397(8)	2.389(4)	2.377(4)	2.364(4)
Ln1-O2	2.396(9)	2.392(5)	2.381(5)	2.362(5)
Ln1-O3	2.381(8)	2.374(4)	2.358(4)	2.351(4)
Ln1-O4	2.506(8)	2.512(4)	2.507(4)	2.509(4)
Ln1-O5	2.369(10)	2.321(4)	2.312(5)	2.300(5)
Ln1-O6	2.370(8)	2.354(4)	2.344(4)	2.335(5)
Ln1-O7	2.339(8)	2.334(5)	2.311(5)	2.308(5)
Ln1-O8	2.425(9)	2.418(4)	2.405(4)	2.400(4)

Ln1-N3	2.795(8)	2.854(2)	2.858(5)	2.871(5)
Ln2-O9	2.387(7)	2.385(4)	2.376(4)	2.357(5)
Ln2-O10	2.421(9)	2.393(5)	2.363(5)	2.361(5)
Ln2-O11	2.350(9)	2.325(4)	2.316(4)	2.385(5)
Ln2-O12	2.443(6)	2.408(5)	2.390(5)	2.305(4)
Ln2-O13	2.341(7)	2.345(5)	2.328(6)	2.319(6)
Ln2-O14	2.376(8)	2.362(4)	2.344(4)`	2.333(4)
Ln2-O15	2.393(7)	2.366(4)	2.361(4)	2.351(4)
Ln2-O16	2.524(7)	2.507(4)	2.520(4)	2.522(5)
Ln2-N4	2.860(8)	2.788(5)	2.777(5)	2.770(5)
O1-Ln1-O2	75.7(3)	80.59(15)	79.80(15)	80.12(16)
O1-Ln1-O3	79.0(3)	77.50(13)	77.30(14)	77.27(15)
O1-Ln1-O4	130.2(2)	134.66(16)	134.67(17)	134.84(18)
O1-Ln1-O5	138.5(3)	135.02(14)	134.94(15)	134.76(16)
O1-Ln1-O6	143.3(3)	141.67(13)	141.71(13)	141.73(14)
O1-Ln1-O7	92.7(3)	85.93(16)	85.93(17)	85.80(17)
O1-Ln1-O8	71.9(3)	66.76(13)	66.66(14)	66.75(15)
O1-Ln1-N3	64.4(2)	63.43(7)	63.47(13)	63.38(14)
O2-Ln1-O3	87.7(3)	86.77(15)	86.81(15)	86.98(16)
O2-Ln1-O4	66.9(3)	68.32(14)	68.97(15)	68.72(15)
O2-Ln1-O5	138.8(3)	138.25(15)	139.02(16)	138.66(16)
O2-Ln1-O6	89.2(3)	88.44(16)	89.10(16)	88.85(17)
O2-Ln1-O7	137.9(3)	137.08(14)	136.70(14)	137.07(14)
O2-Ln1-O8	67.5(3)	65.60(15)	65.00(16)	65.32(16)
O2-Ln1-N3	134.9(2)	137.08(8)	136.62(14)	136.79(15)
O3-Ln1-O4	68.2(3)	68.85(13)	69.18(14)	69.46(15)
O3-Ln1-O5	80.5(3)	82.64(15)	82.59(16)	82.18(16)
O3-Ln1-O6	134.5(3)	138.76(13)	138.98(14)	139.02(15)
O3-Ln1-O7	130.3(3)	129.64(15)	129.51(15)	129.03(16)
O3-Ln1-O8	145.4(3)	137.31(16)	137.01(16)	137.23(17)
O3-Ln1-N3	65.5(3)	64.25(7)	64.15(13)	63.99(15)
O4-Ln1-O5	72.1(3)	70.19(15)	70.25(16)	70.11(17)
O4-Ln1-O6	68.9(3)	71.34(15)	71.29(15)	71.08(16)
O4-Ln1-O7	137.1(3)	139.13(16)	139.13(17)	139.08(17)
O4-Ln1-O8	118.5(3)	122.71(13)	122.52(14)	122.51(15)
O4-Ln1-N3	126.0(2)	121.99(7)	122.07(13)	122.20(14)
O5-Ln1-O6	72.6(3)	74.16(14)	74.19(15)	74.48(16)
O5-Ln1-O7	74.2(3)	76.44(16)	76.52(16)	76.63(16)
O5-Ln1-O8	134.1(3)	139.57(17)	139.89(17)	140.05(18)
O5-Ln1-N3	74.3(2)	71.72(7)	71.48(14)	71.40(15)
O6-Ln1-O7	76.3(3)	77.46(16)	77.37(16)	77.67(18)
O6-Ln1-O8	71.4(3)	75.23(14)	75.40(14)	75.32(15)
O6-Ln1-N3	135.6(2)	134.21(7)	134.07(13)	134.14(14)
O7-Ln1-O8	70.5(3)	71.62(16)	71.78(16)	71.85(16)
O7-Ln1-N3	66.8(2)	65.78(7)	65.70(14)	65.42(15)
O8-Ln1-N3	115.4(3)	114.77(7)	114.90(14)	114.81(15)
O9-Ln2-O10	80.5(3)	74.91(14)	75.36(15)	75.40(16)
O9-Ln2-O11	85.8(3)	92.83(15)	92.64(15)	71.17(16)
O9-Ln2-O12	67.3(2)	71.75(14)	71.35(15)	92.73(16)
O9-Ln2-O13	134.9(2)	138.45(15)	138.37(16)	138.17(17)
O9-Ln2-O14	142.1(2)	142.85(16)	142.52(17)	142.55(17)
O9-Ln2-O15	77.3(2)	78.56(15)	79.15(16)	79.14(16)
O9-Ln2-O16	134.5(3)	130.50(14)	130.86(14)	130.85(15)
O9-Ln2-N4	63.1(2)	64.78(16)	64.90(17)	65.02(17)
O10-Ln2-O11	136.2(3)	137.63(16)	137.95(16)	66.75(15)

O10-Ln2-O12	65.3(3)	67.05(15)	66.80(15)	138.00(17)
O10-Ln2-O13	139.0(3)	139.25(15)	138.73(16)	138.77(16)
O10-Ln2-O14	88.8(3)	89.33(15)	89.04(16)	88.73(16)
O10-Ln2-O15	87.1(3)	87.36(16)	87.68(16)	87.86(16)
O10-Ln2-O16	69.1(3)	67.65(16)	67.31(17)	67.15(17)
O10-Ln2-N4	136.9(2)	134.56(16)	135.08(16)	135.40(17)
O11-Ln2-O12	71.0(3)	70.60(16)	71.17(17)	71.27(17)
O11-Ln2-O13	76.2(3)	74.52(16)	74.70(16)	135.82(15)
O11-Ln2-O14	77.2(3)	76.33(14)	76.33(15)	71.40(18)
O11-Ln2-O15	130.0(3)	130.52(16)	130.16(16)	144.69(18)
O11-Ln2-O16	139.3(3)	136.67(16)	136.51(16)	117.81(17)
O11-Ln2-N4	66.4(2)	66.81(16)	66.40(16)	115.33(17)
O12-Ln2-O13	138.6(3)	134.73(14)	135.49(15)	74.66(17)
O12-Ln2-O14	75.2(3)	71.13(16)	71.18(17)	76.57(15)
O12-Ln2-O15	137.7(3)	144.72(17)	144.76(17)	130.00(17)
O12-Ln2-O16	123.2(2)	118.22(15)	117.90(16)	136.42(16)
O12-Ln2-N4	115.2(2)	115.61(15)	115.62(16)	66.07(17)
O13-Ln2-O14	73.4(3)	73.33(17)	73.69(17)	74.01(18)
O13-Ln2-O15	83.3(3)	80.49(16)	79.69(16)	79.42(17)
O13-Ln2-O16	70.3(3)	71.69(16)	71.48(16)	71.67(17)
O13-Ln2-N4	71.8(2)	73.94(17)	73.77(17)	73.50(18)
O14-Ln2-O15	138.7(3)	135.06(16)	134.94(16)	134.82(17)
O14-Ln2-O16	71.8(3)	68.62(13)	68.54(14)	68.19(14)
O14-Ln2-N4	134.2(2)	135.76(17)	135.52(17)	135.49(18)
O15-Ln2-O16	68.4(2)	68.76(14)	68.82(15)	69.06(15)
O15-Ln2-N4	63.9(2)	65.51(16)	65.69(16)	65.87(17)
O16-Ln2-N4	121.1(2)	126.03(17)	126.33(17)	126.72(17)

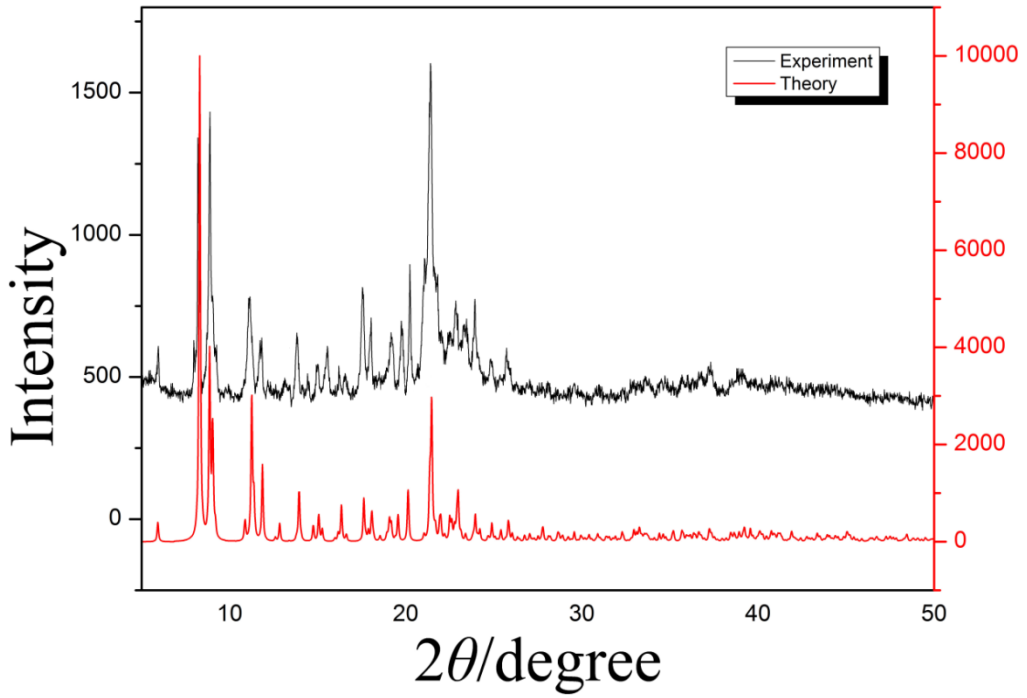

Figure S1 X-ray powder diffraction pattern of compound **1** at room temperature, together with the calculated pattern from the single crystal data.

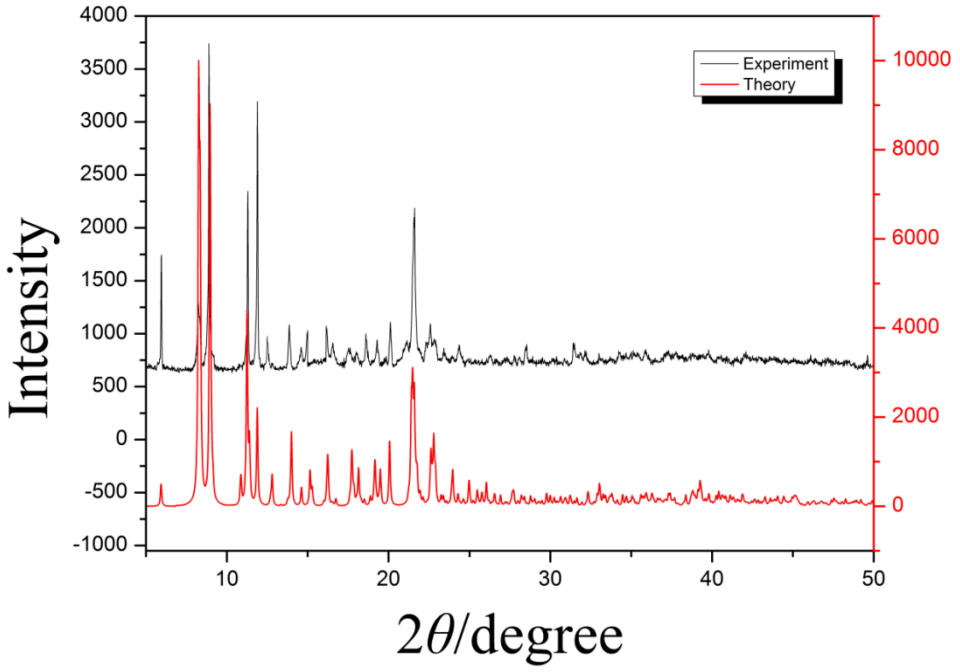

Figure S2 X-ray powder diffraction pattern of compound **2** at room temperature, together with the calculated pattern from the single crystal data.

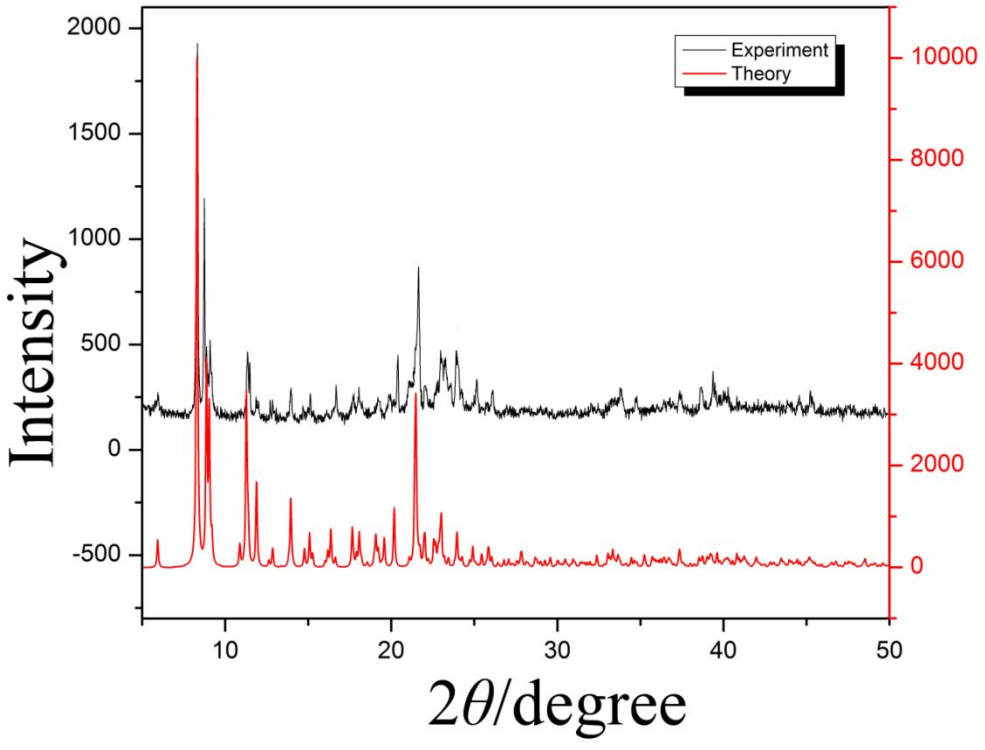

Figure S3 X-ray powder diffraction pattern of compound **3** at room temperature, together with the calculated pattern from the single crystal data.

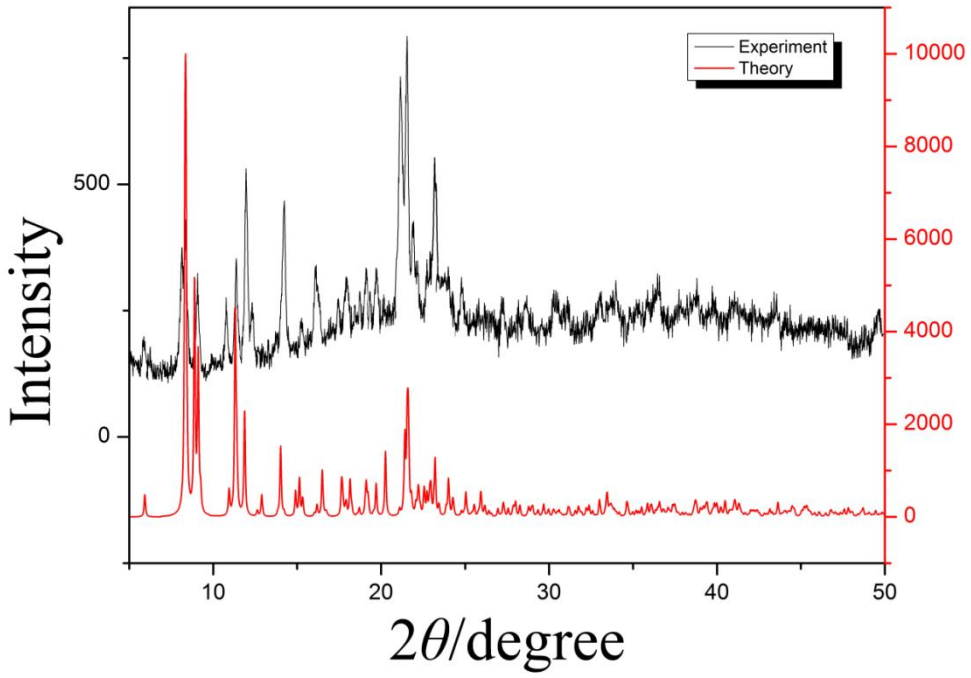

Figure S4 X-ray powder diffraction pattern of compound **4** at room temperature, together with the calculated pattern from the single crystal data.

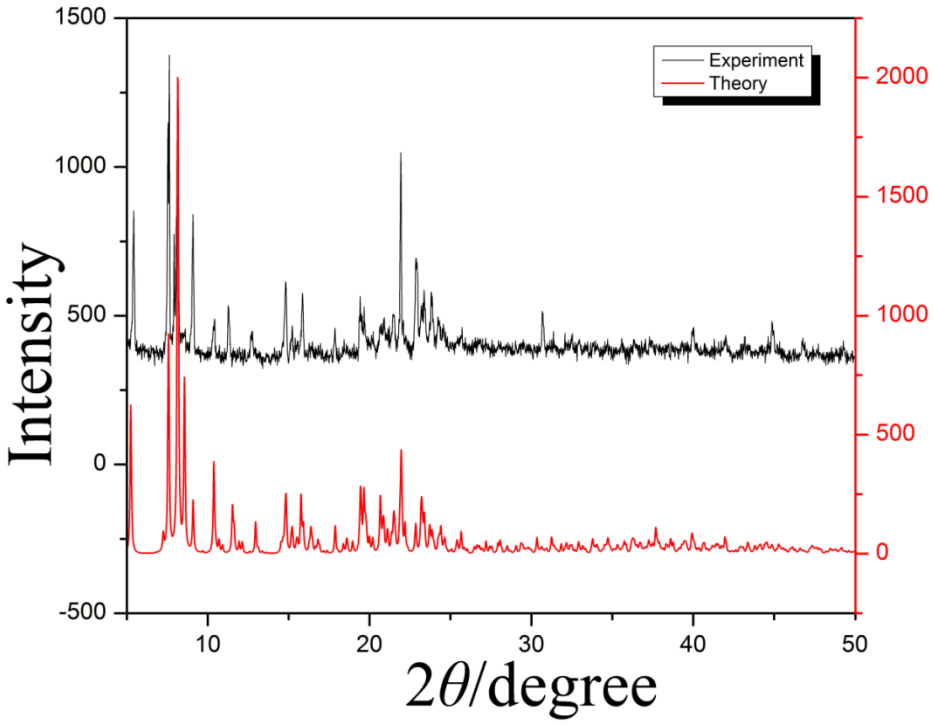

Figure S5 X-ray powder diffraction pattern of compound **5** at room temperature, together with the calculated pattern from the single crystal data.

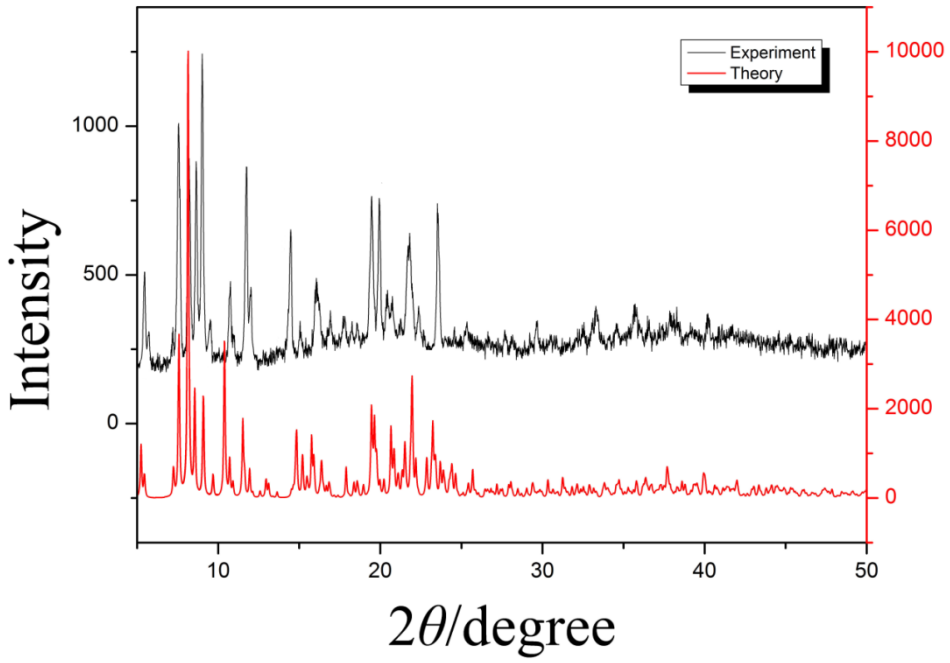

Figure S6 X-ray powder diffraction pattern of compound **6** at room temperature, together with the calculated pattern from the single crystal data.

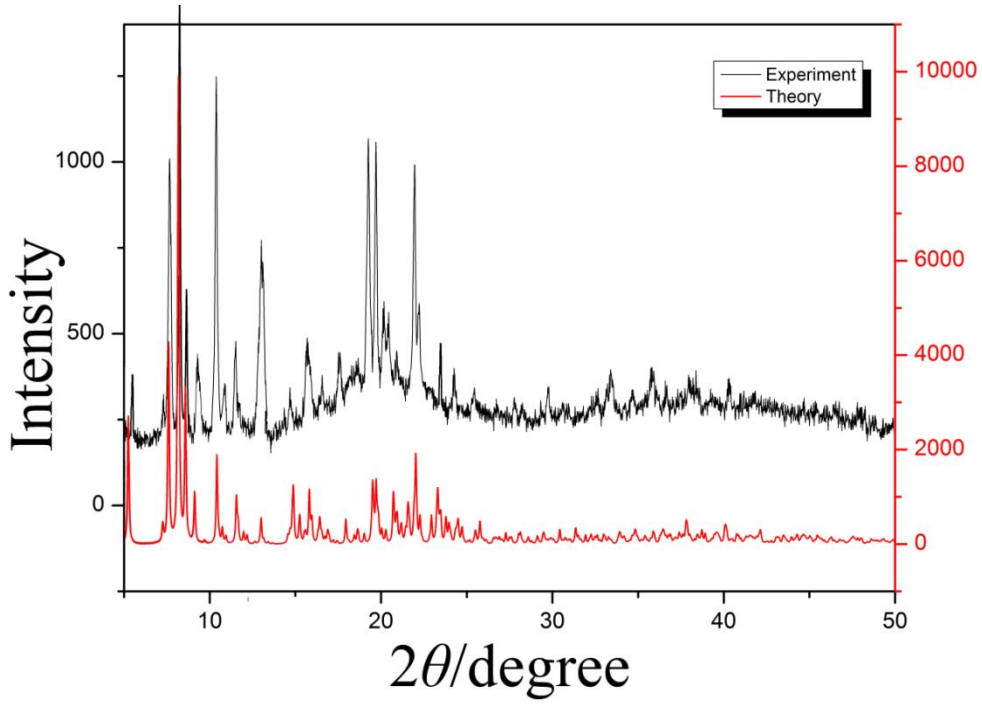

Figure S7 X-ray powder diffraction pattern of compound **7** at room temperature, together with the calculated pattern from the single crystal data.

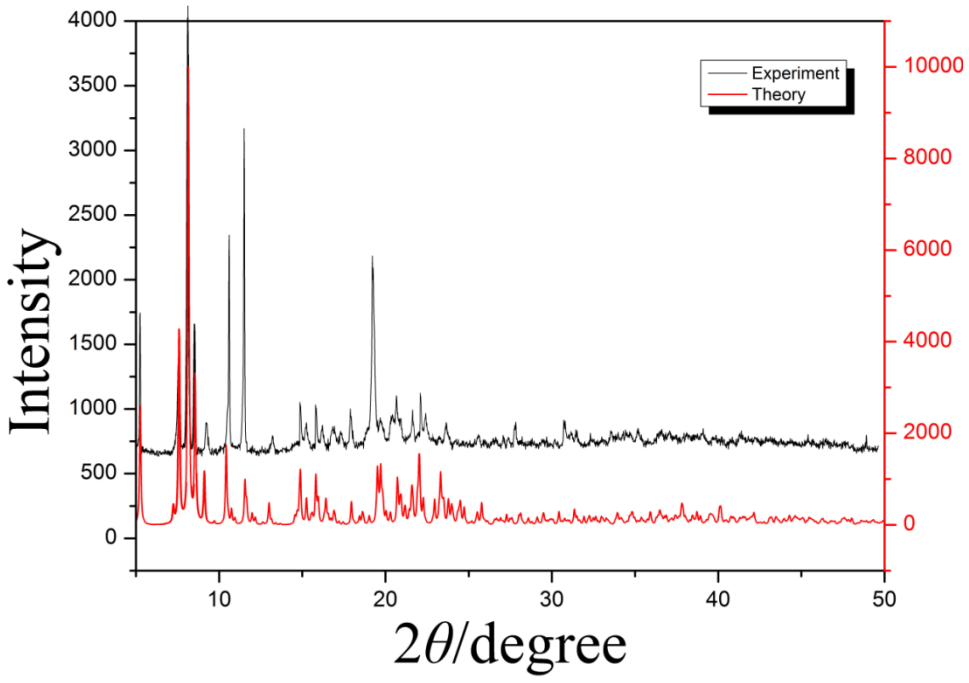

Figure S8 X-ray powder diffraction pattern of compound **8** at room temperature, together with the calculated pattern from the single crystal data.

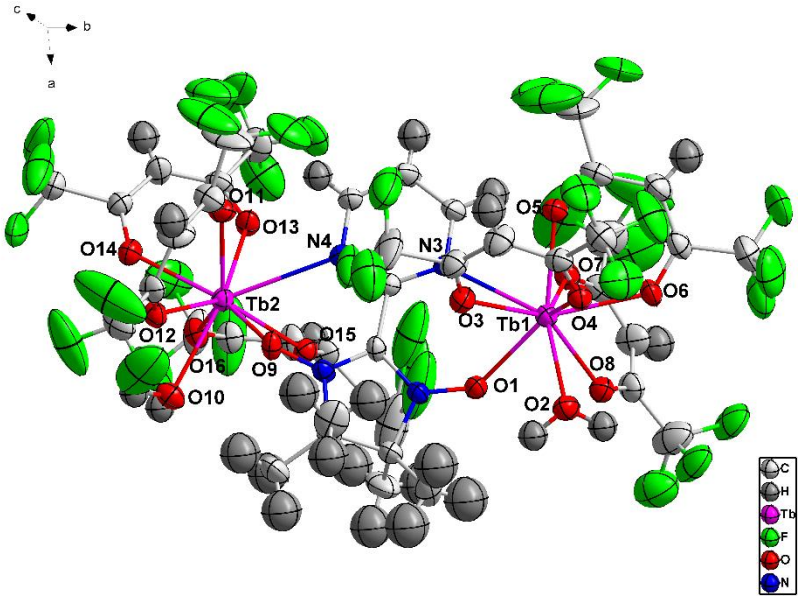

Figure S9 ORTEP view of the asymmetric unit of [(μ-NIT-2-Pm)Tb_2(hfac)$_6$(H_2O)$_2$] with thermal ellipsoids at 30% probability.

Table S3. Continuous Shape Measures calculation for **1-4**.

Structure [ML8]	1(M1)	2(M1)	3(M1)	4(M1)
OP-8	31.171	31.212	31.182	31.456
HPY-8	22.769	23.096	22.940	22.625
HBPY-8	16.120	16.224	16.250	16.195
CU-8	10.924	10.944	10.853	10.782
SAPR-8	1.119	1.292	1.179	1.175
TDD-8	1.404	1.256	1.283	1.309
JGBF-8	14.078	13.672	13.887	14.103
JETBPY-8	28.457	28.576	28.446	28.384
JBTP-8	1.420	1.359	1.394	1.452
BTPR-8	1.376	1.311	1.368	1.412
JSD-8	3.154	2.928	2.979	3.074
TT-8	11.505	11.408	11.328	11.311
ETBPY-8	24.726	25.195	25.001	24.737

OP-8	1	D8h	Octagon
HPY-8	2	C7v	Heptagonal pyramid
HBPY-8	3	D6h	Hexagonal bipyramid
CU-8	4	Oh	Cube
SAPR-8	5	D4d	Square antiprism
TDD-8	6	D2d	Triangular dodecahedron
JGBF-8	7	D2d	Johnson - Gyrobifastigium (J26)
JETBPY-8	8	D3h	Johnson - Elongated triangular bipyramid (J14)
JBTP-8	9	C2v	Johnson - Biaugmented trigonal prism (J50)
BTPR-8	10	C2v	Biaugmented trigonal prism
JSD-8	11	D2d	Snub disphenoid (J84)
TT-8	12	Td	Triakis tetrahedron
ETBPY-8	13	D3h	Elongated trigonal bipyramid (see 8)

Table S4. Continuous Shape Measures calculation for **5-8**.

Structure [ML9]	5(M1)	5(M2)	6(M1)	6(M2)	7(M1)	7(M2)	8(M1)	8(M2)
EP-9	33.417	34.305	33.255	34.074	33.424	34.194	33.615	34.468
OPY-9	23.575	23.025	23.622	23.135	23.618	23.099	23.610	23.176
HBPY-9	20.947	18.969	21.001	19.020	20.962	19.042	20.955	18.742
JTC-9	13.268	14.205	13.330	14.134	13.384	14.120	13.305	14.147
JCCU-9	10.231	9.205	10.143	9.257	10.144	9.259	10.062	9.089
CCU-9	10.156	8.874	10.178	8.973	10.117	8.941	9.961	8.716
JCSAPR-9	1.663	1.739	1.585	1.700	1.594	1.724	1.673	1.784
CSAPR-9	1.314	1.069	1.383	1.069	1.354	1.078	1.348	1.078
JTCTPR-9	1.158	1.484	1.099	1.424	1.424	1.447	1.181	1.540
TCTPR-9	1.159	1.141	1.224	1.208	1.167	1.172	1.123	1.139
JTDIC-9	13.377	13.300	13.460	13.443	13.404	13.334	13.397	13.294
HH-9	11.643	11.261	11.750	11.289	11.741	11.247	11.592	11.065
MFF-9	1.761	1.226	1.824	1.231	1.797	1.239	1.786	1.188

EP-9	1	D9h	Enneagon
OPY-9	2	C8v	Octagonal pyramid
HBPY-9	3	D7h	Heptagonal bipyramid
JTC-9	4	C3v	Triangular cupola (J3) = trivacant cuboctahedron
JCCU-9	5	C4v	Capped cube (Elongated square pyramid, J8)
CCU-9	6	C4v	Capped cube
JCSAPR-9	7	C4v	Capped sq. antiprism (Gyroelongated square pyramid J10)
CSAPR-9	8	C4v	Capped square antiprism
JTCTPR-9	9	D3h	Tricapped trigonal prism (J51)
TCTPR-9	10	D3h	Tricapped trigonal prism
JTDIC-9	11	C3v	Tridiminished icosahedron (J63)
HH-9	12	C2v	Hula-hoop
MFF-9	13	Cs	Muffin

2. Magnetic Property

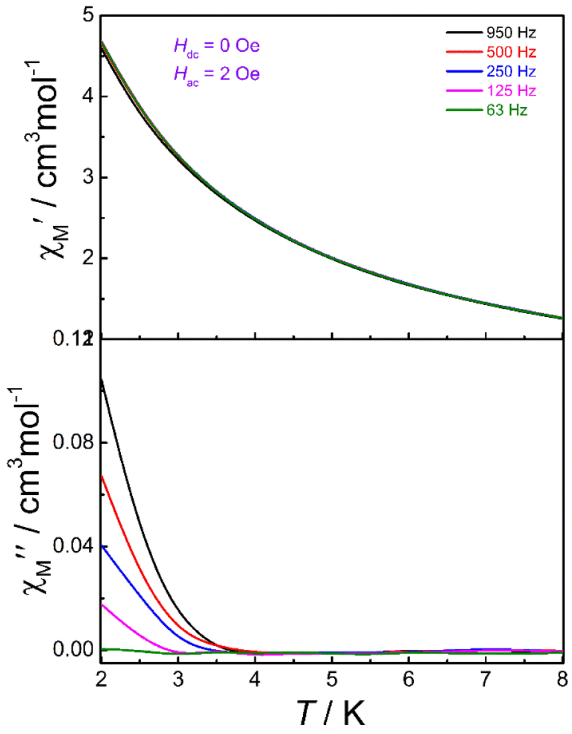

Figure S10 Temperature dependent in-phase (top) and out-of-phase (bottom) a.c. susceptibility data for **1** measured under 0 Oe dc field (H_{ac} = 2 Oe).

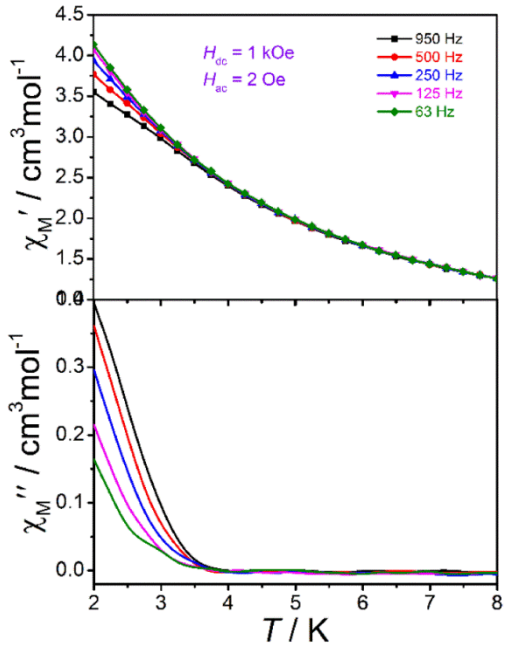

Figure S11 Temperature dependent in-phase (top) and out-of-phase (bottom) a.c. susceptibility data for **1** measured under 1 kOe dc field (H_{ac} = 2 Oe).

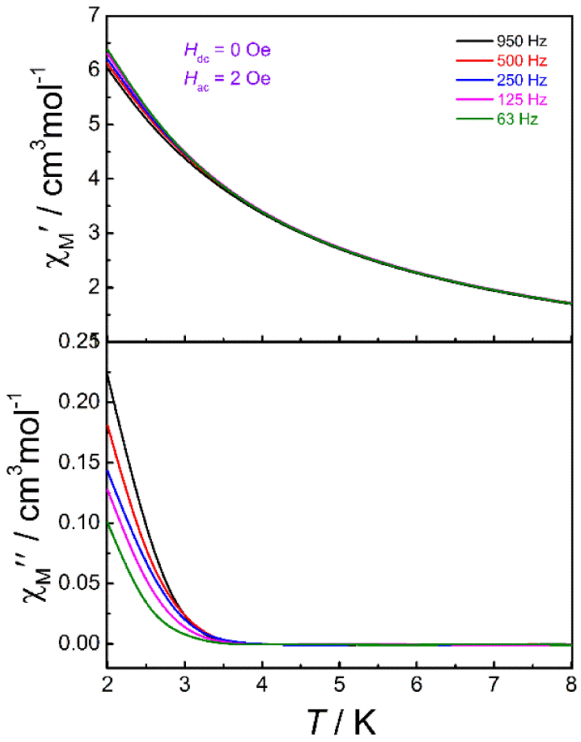

Figure S12 Temperature dependent in-phase (top) and out-of-phase (bottom) a.c. susceptibility data for **3** measured under 0 Oe dc field (H_{ac} = 2 Oe).

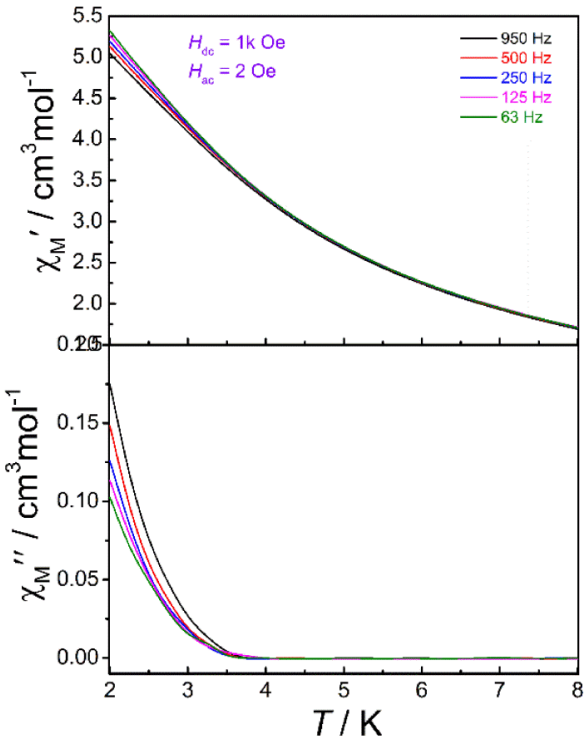

Figure S13 Temperature dependent in-phase (top) and out-of-phase (bottom) a.c. susceptibility data for **3** measured under 1 kOe dc field (H_{ac} = 2 Oe).

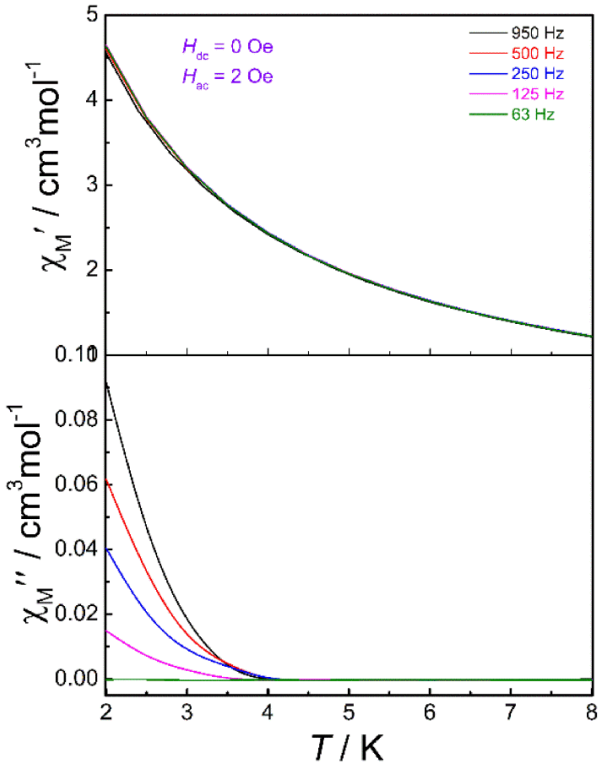

Figure S14 Temperature dependent in-phase (top) and out-of-phase (bottom) a.c. susceptibility data for **4** measured under 0 Oe dc field (H_{ac} = 2 Oe).

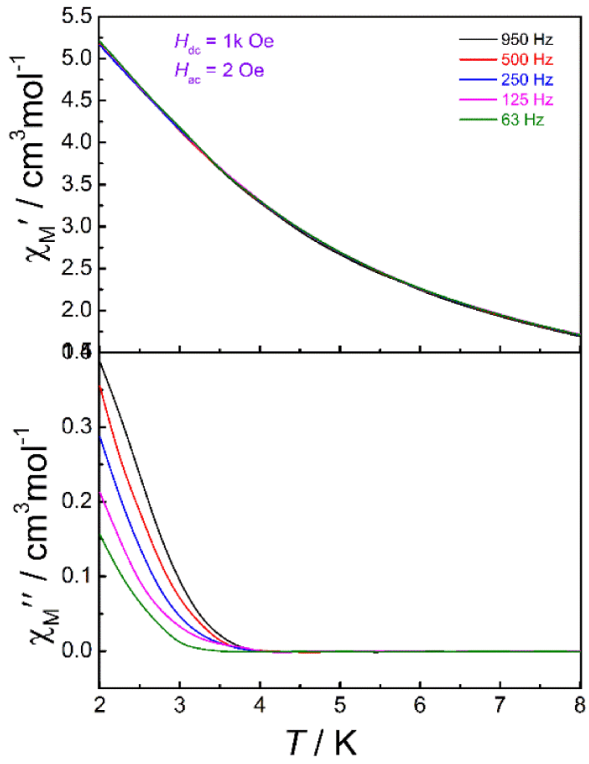

Figure S15 Temperature dependent in-phase (top) and out-of-phase (bottom) a.c. susceptibility data for **4** measured under 1 kOe dc field (H_{ac} = 2 Oe).

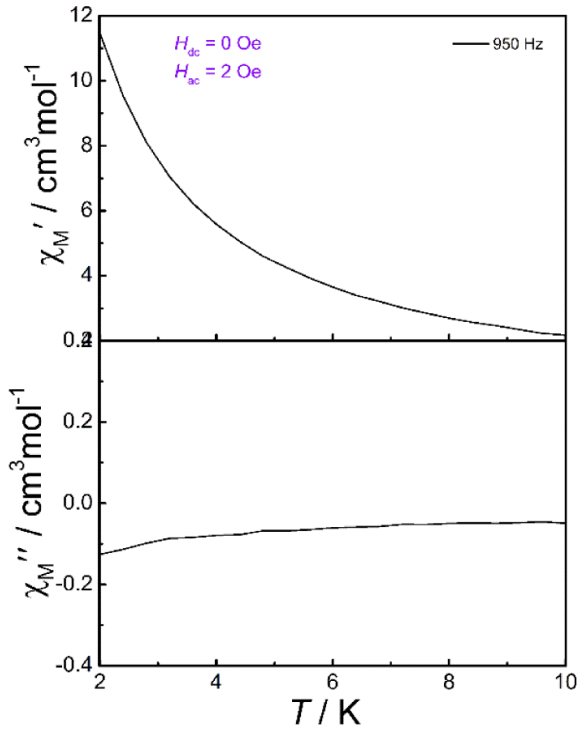

Figure S16 Temperature dependent in-phase (top) and out-of-phase (bottom) a.c. susceptibility data for **5** measured under 0 Oe dc field (H_{ac} = 2 Oe). No out-of-phase signals or frequency dependence were observed above 2.0 K.

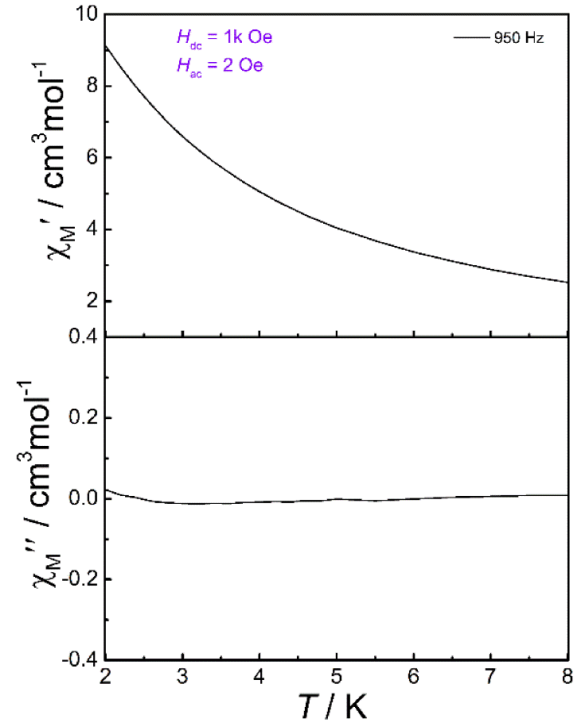

Figure S17 Temperature dependent in-phase (top) and out-of-phase (bottom) a.c. susceptibility data for **5** measured under 1 kOe dc field (H_{ac} = 2 Oe). No out-of-phase signals or frequency dependence were observed above 2.0 K.

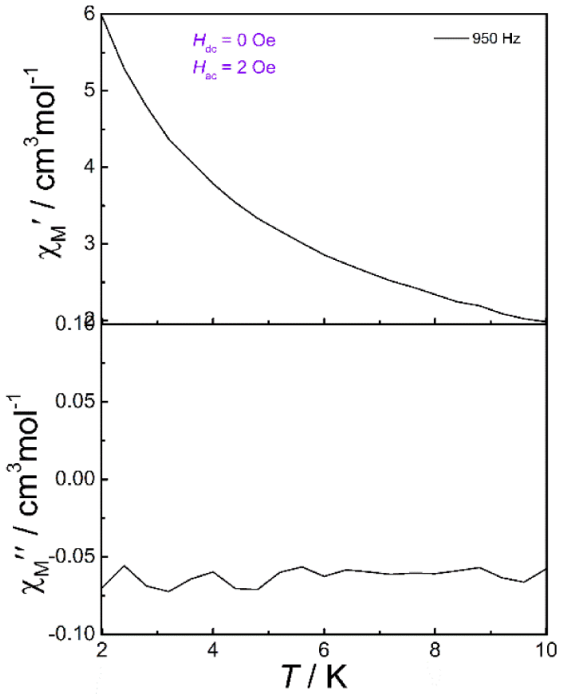

Figure S18 Temperature dependent in-phase (top) and out-of-phase (bottom) a.c. susceptibility data for **7** measured under 0 Oe dc field (H_{ac} = 2 Oe). No out-of-phase signals or frequency dependence were observed above 2.0 K.

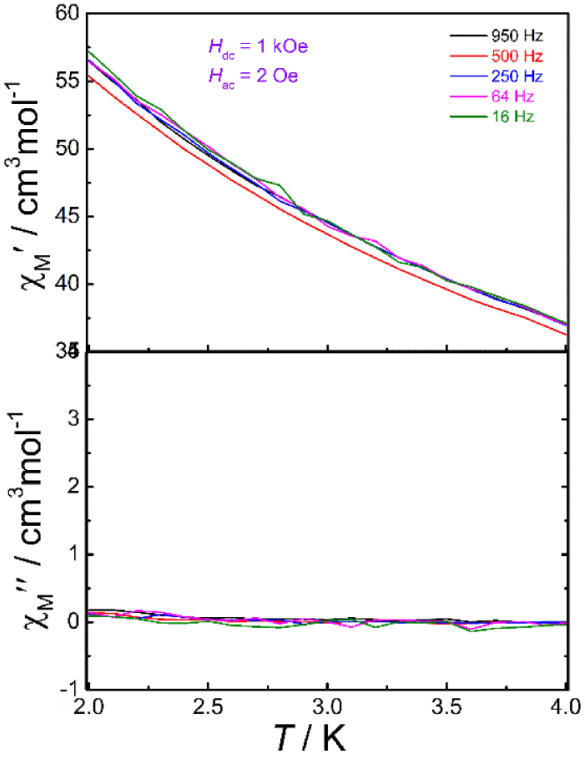

Figure S19 Temperature dependent in-phase (top) and out-of-phase (bottom) a.c. susceptibility data for **7** measured under 1 kOe dc field (H_{ac} = 2 Oe). No out-of-phase signals or frequency dependence were observed above 2.0 K.

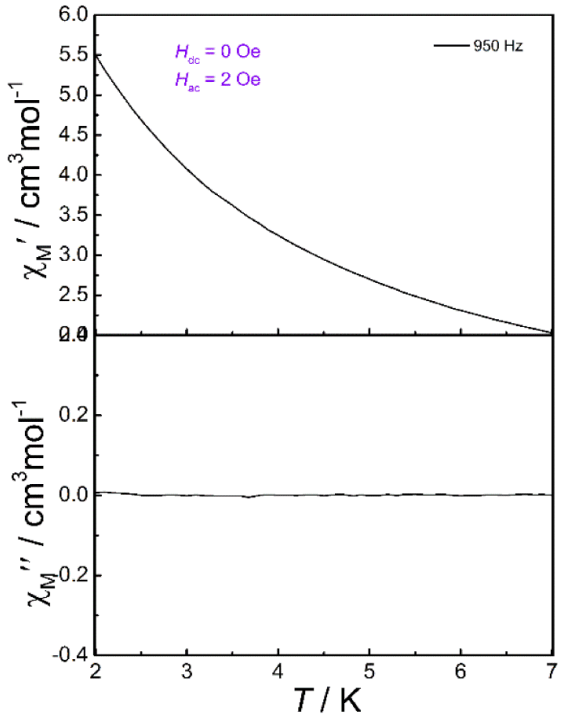

Figure S20 Temperature dependent in-phase (top) and out-of-phase (bottom) a.c. susceptibility data for **8** measured under 0 Oe dc field (H_{ac} = 2 Oe). No out-of-phase signals or frequency dependence were observed above 2.0 K.

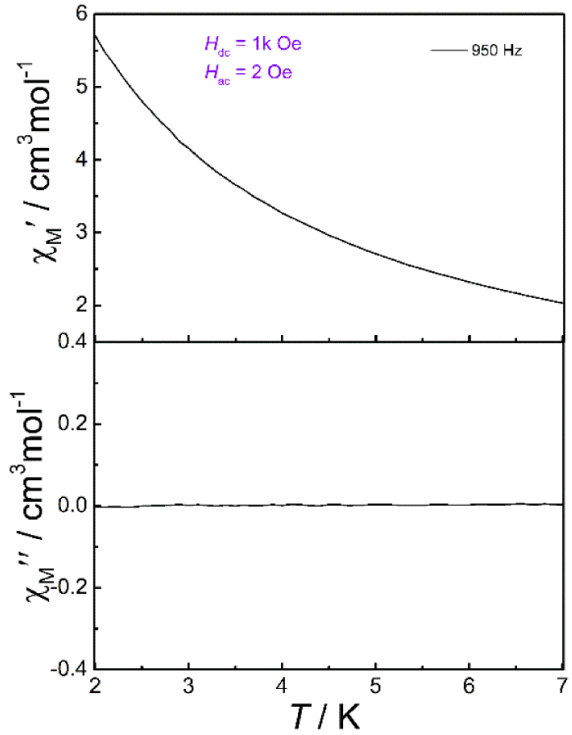

Figure S21 Temperature dependent in-phase (top) and out-of-phase (bottom) a.c. susceptibility data for **8** measured under 1 kOe dc field (H_{ac} = 2 Oe). No out-of-phase signals or frequency dependence were observed above 2.0 K.

3. Theoretical calculations

Ab initio calculation on individual lanthanide fragment

Considering the similar coordination environment around two Ln^{III} ions for complexes **5**–**8**, we only calculate one type of Ln^{III} (Tb^{III}, Dy^{III}, Ho^{III} or Er^{III}) fragment for each of them. Complete-active-space self-consistent field (CASSCF) calculations on the individual Ln^{III} (Tb^{III}, Dy^{III}, Ho^{III} or Er^{III}) fragment (see Figure S22 for the complete structure of complex **1**; see Figure S23 for the other seven Ln^{III} fragments) of complexes **1**–**8** on the basis of X-ray determined geometry have been carried out with MOLCAS 8.0 program package.[1] For CASSCF calculations, the basis sets for all atoms are atomic natural orbitals from the MOLCAS ANO-RCC library: ANO-RCC-VTZP for Ln^{III} (Tb^{III}, Dy^{III}, Ho^{III} or Er^{III}); VTZ for close O and N; VDZ for distant atoms. The calculations employed the second order Douglas-Kroll-Hess Hamiltonian, where scalar relativistic contractions were taken into account in the basis set and the spin-orbit coupling was handled separately in the restricted active space state interaction (RASSI-SO) procedure. The active electrons in 7 active spaces include all *f* electrons (CAS(8 in 7) for Tb^{III} (**1** and **5**), CAS(9 in 7) for Dy^{III} (**2** and **6**), CAS(10 in 7) for Ho^{III} (**3** and **7**) and CAS(11 in 7) for Er^{III} (**4** and **8**) in the CASSCF calculation. To exclude all the doubts, we calculated all the roots in the active space. We have mixed the maximum number of spin-free state which was possible with our hardware (all from 7 septets, all from 140 quintets and 68 from 500 triplets for the Tb^{III} fragment; all from 21 sextets, 128 from 224 quadruplets and 130 from 490 doublets for Dy^{III} fragments; all from 35 quintets, 150 from 210 triplets and 120 from 196 singlets for the Ho^{III} fragment; all from 35 quadruplets, all from 112 doublets for Er^{III} fragment). The calculated several lowest calculated Kramers doublets (KDs) and the ***g*** tensors of complexes **1**–**8** using CASSCF/RASSI are shown in Table S5. The orientations of the local main magnetic axes of the ground Kramers doublets on Ln^{III} (Tb^{III}, Dy^{III}, Ho^{III} or Er^{III}) of complexes **1**–**8** were shown in Figure S23.

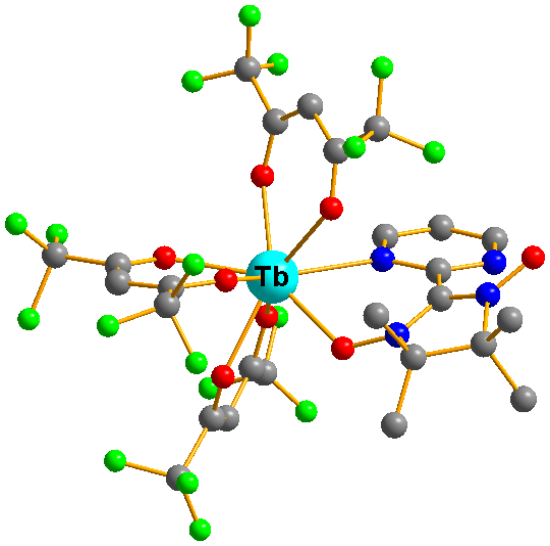

Figure S22. Calculated complete structure of the Tb^{III} fragment of complex **1**; H atoms are omitted.

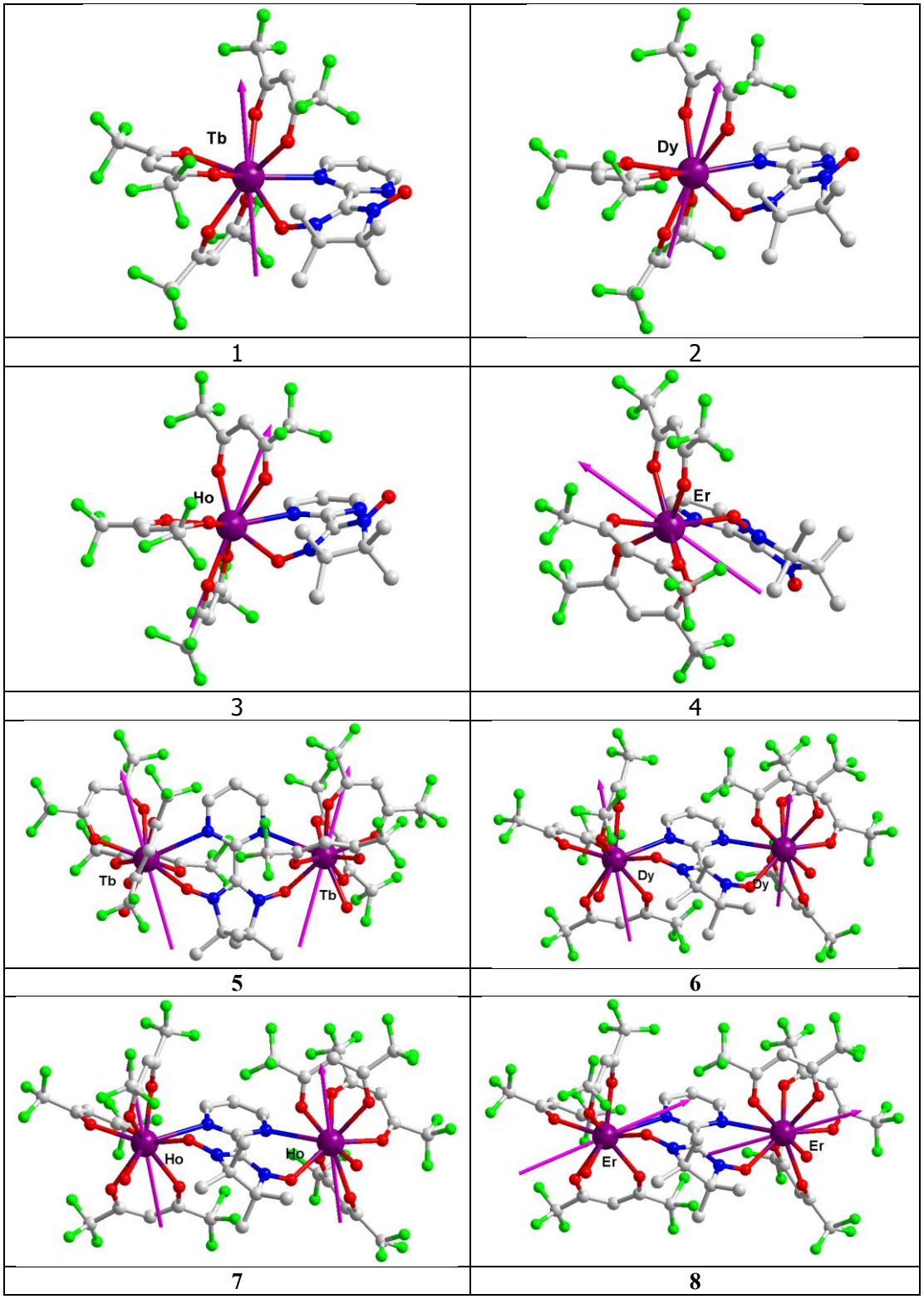

Figure S23. Orientations of the local main magnetic axes of the ground Kramers doublet on Ln^{III} (Tb^{III}, Dy^{III}, Ho^{III} or Er^{III}) of complexes **1**–**8**.

Table S5. Calculated energy levels (cm^{-1}), ***g*** (g_x, g_y, g_z) tensors and m_J values of the Kramers doublets (KDs) of the individual Ln^{III} (Tb^{III}, Dy^{III}, Ho^{III} or Er^{III}) fragments of complexes **1**–**8**.

KDs	**1(Tb)**			**2(Dy)**			**3(Ho)**			**4(Er)**		
	E/cm^{-1}	***g***	m_J	E/cm^{-1}	***g***	m_J	E/cm^{-1}	***g***	m_J	E/cm^{-1}	***g***	m_J
1	0.0 0.6	0.000 0.000 17.471	±6	0.0	0.013 0.019 19.044	±15/2	0.0 0.1	0.000 0.000 17.962	±8	0.0	1.303 6.299 12.047	±15/2
2	36.1 37.8	0.000 0.000 16.575	±2	98.1	0.280 0.416 15.062	±13/2	44.4 46.5	0.000 0.000 15.957	±1	31.6	0.512 0.934 12.342	±11/2
3	102.1 115.3	0.000 0.000 12.348	±3	163.1	1.444 1.962 11.631	±9/2	78.1 85.5	0.000 0.000 11.594	±6	49.5	0.106 2.738 10.742	±9/2
4	152.8		0	207.9	0.182 2.708 9.500	±7/2	112.1 116.8	0.000 0.000 11.334	±2	75.4	1.378 1.761 12.537	±5/2
5	189.2 205.6	0.000 0.000 13.806	±5	251.8	3.741 5.379 10.052	±3/2	159.2		0	139.3	0.917 3.288 8.868	±7/2
6	240.5 244.2	0.000 0.000 13.121	±1	297.4	1.205 2.990 14.993	±1/2	178.3 190.3	0.000 0.000 10.080	±5	186.1	0.238 1.522 10.431	±3/2
7	417.9 418.2	0.000 0.000 17.521	±4	388.6	0.003 0.065 19.464	±11/2	197.7 212.5	0.000 0.000 7.495	±3	226.1	0.746 1.406 13.255	±1/2
8				428.7	0.061 0.099 19.463	±5/2	218.3 224.7	0.000 0.000 10.713	±4	287.9	0.034 0.106 16.036	±13/2
9							241.6 250.7	0.000 0.000 15.582	±7			
KDs	**5(Tb)**			**6(Dy)**			**7(Ho)**			**8(Er)**		

	E/cm^{-1}	g	m_J	E/cm^{-1}	g	m_J	E/cm^{-1}	g	m_J	E/cm^{-1}	g	m_J
1	0.0 0.6	0.000 0.000 17.096	±6	0.0	0.007 0.012 19.669	±15/2	0.0 5.0	0.000 0.000 15.631	±8	0.0	0.551 1.178 15.229	±15/2
2	19.1 20.5	0.000 0.000 16.616	±4	154.6	0.323 0.645 16.019	±13/2	23.2 40.3	0.000 0.000 12.434	±7	41.5	9.182 6.134 1.719	±3/2
3	76.6 93.3	0.000 0.000 11.927	±5	207.4	0.285 1.341 12.308	±11/2	61.8		0	66.6	0.228 3.857 10.430	±11/2
4	123.5		±1	234.1	3.167 4.806 12.975	±3/2	80.6 83.0	0.000 0.000 8.824	±5	97.1	0.251 3.088 10.040	±9/2
5	176.9 189.5	0.000 0.000 11.937	±3	252.7	1.751 3.066 13.086	±9/2	116.3 127.9	0.000 0.000 12.744	±3	153.2	1.966 4.458 10.755	±13/2
6	261.7 265.4	0.000 0.000 15.282	±2	285.8	1.276 3.043 11.386	±5/2	162.8 166.3	0.000 0.000 11.379	±6	195.0	1.674 5.033 8.699	±5/2
7	306.1 306.9	0.000 0.000 17.145	0	304.2	0.726 4.195 13.104	±7/2	183.1 196.2	0.000 0.000 11.614	±1	244.4	1.385 2.413 11.239	±7/2
8				468.4	0.010 0.020 19.665	±1/2	215.1 226.9	0.000 0.000 14.188	±4	278.5	0.435 2.808 13.734	±1/2
9							260.5 262.7	0.000 0.000 16.970	±2			

Fitting the exchange interaction in complexes 1-8 using Lines model based on the CASSCF results

To fit the exchange interactions in these eight complexes, we took two steps. Firstly, we calculated the mononuclear fragments using CASSCF to obtain the corresponding magnetic properties (see above). And then, the exchange interaction between the magnetic centers is considered within the Lines model,[2] while the account of the dipole-dipole magnetic coupling is treated exactly. The Lines model is effective and has been successfully used widely in the research field of binuclear lanthanide single-molecule magnets.[3]

For complexes **1**–**4**, the exchange Hamiltonian is:

$$\widehat{H}_{exch} = -J^{total}_{Ln-\mathrm{Radical}}\,\hat{\tilde{S}}_{Ln}\,\hat{\tilde{S}}_{\mathrm{Radical}} \qquad (1)$$

For complexes **5**–**8**, the exchange Hamiltonian is:

$$\widehat{H}_{exch} = -J^{total}_{Ln-\mathrm{Radical}}(\hat{\tilde{S}}_{Ln1}\,\hat{\tilde{S}}_{\mathrm{Radical}} + \hat{\tilde{S}}_{Ln2}\,\hat{\tilde{S}}_{\mathrm{Radical}}) - J^{total}_{Ln-Ln}\,\hat{\tilde{S}}_{Ln1}\,\hat{\tilde{S}}_{Ln2} \qquad (2)$$

The $J^{total}_{Ln-\mathrm{Radical}}$ and J^{total}_{Ln-Ln} are parameters of the total magnetic interaction ($J^{total} = J^{diploar} + J^{exchange}$) between Ln-Radical and Ln1-Ln2, respectively. The $\hat{\tilde{S}}_{Ln}$ = ±1/2 are the ground pseudospins on the Ln^{III} sites and the radical. The radicals in eight complexes were considered as isotropic, and the average *g* values were all set as 2.0 during the fitting. The total coupling constants were fitted through comparison of the computed and measured magnetic susceptibilities using the POLY_ANISO program.[4] The intermolecular interactions *zJ´* of **1–8** were fitted to be –0.01, 0.03, –0.01, 0.03, –0.01, 0.01, –0.05 and –0.05 cm^{-1}, respectively. Based on these results, the obtained exchange energies (cm^{-1}) and tunneling gaps (μ_B) for the lowest several exchange doublets of **1–8** were listed in Table S6.

Table S6. Exchange energies (cm^{-1}), and tunneling gaps (μ_B)for the lowest several exchange doublets of **1**–**8**.

	1(Tb)		**2(Dy)**		**3(Ho)**		**4(Er)**	
	E	Δ_{tun}	*E*	Δ_{tun}	*E*	Δ_{tun}	*E*	Δ_{tun}
1	0.000	0.65	0.000	0.16E-03	0.000	0.59	0.000	0.25E-01
2	0.604	0.65	0.094	0.29E-04 1→2- 0.52E-01	0.162	0.59	0.044	0.16E-01 1→2- 1.52

	5(Tb)		**6(Dy)**		**7(Ho)**		**8(Er)**	
	E	Δ_{tun}	*E*	Δ_{tun}	*E*	Δ_{tun}	*E*	Δ_{tun}
1	0.000	0.51	0.000	0.18E-05	0.000	0.66	0.000	0.28E-01
2	0.333	0.51	0.194	0.14E-05	0.966	0.66	0.101	0.96E-01
3	1.581	0.66	0.333	0.67	1.061	0.66	0.114	0.72
4	1.841	0.66	0.333	0.67	1.727	0.66	0.114	0.66

Reference

(1) Karlström, G.; Lindh, R.; Malmqvist, P. -Å.; Roos, B. O.; Ryde, U.; Veryazov, V.; Widmark, P. -O.; Cossi, M.; Schimmelpfennig, B.; Neograd y, P.; Seijo, L. MOLCAS: a Program Package for Computational Chemistry. *Comput. Mater. Sci*. **2003**, *28*, 222.

(2) Lines, M. E. *J. Chem. Phys*. **1971**, *55*, 2977.

(3) (a) Mondal, K. C.; Sundt, A.; Lan, Y. H.; Kostakis, G. E.; Waldmann, O.; Ungur, L.; Chibotaru, L. F.; Anson, C. E.; Powell, A. K. *Angew. Chem. Int. Ed*. **2012**, *51*, 7550. (b) Langley, S. K.; Wielechowski, D. P.; Vieru, V.; Chilton, N. F.; Moubaraki, B.; Abrahams, B. F.; Chibotaru, L. F.; Murray, K. S. *Angew. Chem. Int. Ed*. **2013**, *52*, 12014.

(4) (a) Chibotaru, L. F.; Ungur, L.; Soncini, A. *Angew. Chem. Int. Ed.*, **2008**, *47*, 4126. (b) Ungur, L.; Van den Heuvel, W.; Chibotaru, L. F. *New J. Chem.*, **2009**, *33*, 1224. (c) Chibotaru, L. F.; Ungur, L.; Aronica, C.; Elmoll, H.; Pilet, G.; Luneau, D. *J. Am. Chem. Soc.*, **2008**, *130*, 12445.